Adv. Radio Sci., 4, 73–78, 2006
www.adv-radio-sci.net/4/73/2006/

Advances in Radio Science

Coherent and non-coherent processing of multiband radar sensor data

S. Tejero, U. Siart, and J. Detlefsen

Institute for High Frequency Engineering, Technische Universität München, D-80290 München, Munich, Germany

Abstract. Increasing resolution is an attractive goal for all types of radar sensor applications. Obtaining high radar resolution is strongly related to the signal bandwidth which can be used. The currently available frequency bands however, restrict the available bandwidth and consequently the achievable range resolution. As nowadays more sensors become available e.g. on automotive platforms, methods of combining sensor information stemming from sensors operating in different and not necessarily overlapping frequency bands are of concern. It will be shown that it is possible to derive benefit from perceiving the same radar scenery with two or more sensors in distinct frequency bands. Beyond ordinary sensor fusion methods, radar information can be combined more effectively if one compensates for the lack of mutual coherence, thus taking advantage of phase information.

At high frequencies, complex scatterers can be approximately modeled as a group of single scattering centers with constant delay and slowly varying amplitude, i.e. a set of complex exponentials buried in noise. The eigenanalysis algorithms are well known for their capability to better resolve complex exponentials as compared to the classical spectral analysis methods. These methods exploit the statistical properties of those signals to estimate their frequencies. Here, two main approaches to extend the statistical analysis for the case of data collected at two different subbands are presented. One method relies on the use of the band gap information (and therefore, coherent data collection is needed) and achieves an increased resolution capability compared with the single-band case. On the other hand, the second approach does not use the band gap information and represents a robust way to process radar data collected with incoherent sensors. Combining the information obtained with these two approaches a robust estimator of the target locations with increased resolution can be built.

Correspondence to: S. Tejero (simon.tejero@tum.de)

1 Introduction

Increasing resolution is an attractive goal for all types of radar sensor applications. Obtaining high radar resolution is strongly related to the signal bandwidth which can be used. The currently available frequency bands however, restrict the available bandwidth and consequently the achievable range resolution. As nowadays more sensors become available e.g. on automotive platforms, methods of combining sensor information stemming from sensors operating in different and not necessarily overlapping frequency bands are of concern. Beyond ordinary sensor fusion methods, radar information can be combined more effectively if one compensates for the lack of mutual coherence, thus taking advantage of phase information.

In this article, the possibility to obtain a benefit in the radar performance by exploiting the availability of sensors operating at different frequency bands will be analyzed. We will concentrate on the dualband case, i.e. two sensors which observe the same radar scenario from the same aspect angle.

2 Radar signal model

In the common frequency bands for radar systems the targets can be considered to be in the high frequency range, as they usually are greater than a wavelength. Some very popular high frequency approximations for solving scattering problems are the Geometrical Optics (GO) theory and one of its extensions, the Geometrical Theory of Diffraction (GTD) (Hansen, 1981; James, 1986; McNamara et al., 1990). Both approximations are based in the decomposition of a scatterer in a set of individual scattering centers with a specific frequency dependence. These scattering centers corresponds to specular reflections, diffraction at wedges or tips or creeping wave terms. Assuming that the high frequency approximation is valid, the radar response of a target or a group of them

Published by Copernicus GmbH on behalf of the URSI Landesausschuss in der Bundesrepublik Deutschland e.V.

can be represented as a sum of individual scattering centers with constant delay:

$$X(t) = \sum_{p=1}^{P} A_p \delta(t - \tau_p) \tag{1}$$

where each Dirac's delta represents a scattering center at distance $c_0\tau_i/2$ with amplitude α_i. In the high-frequency range this model is valid for a wide frequency band, so that the expression for the frequency domain results in

$$x(f) = \sum_{p=1}^{P} A_p e^{j2\pi f \tau_p}. \tag{2}$$

This radar response is sampled by a system working at a frequency band $\mathcal{B}_l$ and can be expressed as:

$$x_l[n] = \sum_{p=1}^{P} A_p z_p^{k_{0l}+n} = \sum_{p=1}^{P} a_{pl} z_p^n \tag{3}$$

where

$$z_p = e^{j\Omega_p}$$
$$\Omega_p = \Delta\omega\tau_p$$
$$a_{pl} = A_p e^{j\omega_{0l}\tau_p}$$

and τ_p is the round trip time, $\Delta\omega$ the angular frequency increment and ω_{0l} is the angular start frequency for band $\mathcal{B}_l$.

3 Radar signal processing

Analyzing Eqs. (2) and (3) it can be noted that the radar problem of finding the position of the scattering centers in the frequency radar response is equivalent to the estimation of the frequencies of complex exponentials in a time domain signal or the angles of the poles z_p. Therefore, spectral or frequency estimation algorithms can be applied. In this paper, the dualband analysis is based on the Multiple Signal Classification (MUSIC) algorithm, but the results can be extended to other parametrized spectral estimation techniques, like Autoregressive (AR) algorithms, as well.

3.1 Single-band MUSIC

A short review of the MUSIC algorithm for a single-band dataset is given here, further information can be found in the literature (Marple, 1987; Schmidt, 1986). Assume the radar frequency response of Eq. (3) is received in the presence of complex white Gaussian Noise (CWGN) $w[n]$ in the frequency band $\mathcal{B}$

$$y[n] = \sum_{p=1}^{P} a_p z_p^n + w[n], \quad n = 0, \ldots, N-1$$
$$y[n] = x[n] + w[n]. \tag{4}$$

With the samples of the data sequence $x[n]$, the so called data matrix $\mathbf{X}$ of order L –equal to the data matrix in the AR covariance method– can be built and decomposed into the matrices $\mathbf{B}$ and $\mathbf{C}$:

$$\mathbf{X} = \begin{bmatrix} x[L-1] & x[L-2] & \cdots & x[0] \\ x[L] & x[L-1] & \cdots & x[1] \\ \vdots & \vdots & \ddots & \vdots \\ x[N-1] & x[N-2] & \cdots & x[N-L] \end{bmatrix} = \mathbf{B} \cdot \mathbf{C} \tag{5}$$

$$\mathbf{B} = \begin{bmatrix} a_1 z_1^{L-1} & a_2 z_2^{L-1} & \cdots & a_P z_P^{L-1} \\ a_1 z_1^{L} & a_2 z_2^{L} & \cdots & a_P z_P^{L} \\ \vdots & \vdots & \ddots & \vdots \\ a_1 z_1^{N-1} & a_2 z_2^{N-1} & \cdots & a_P z_P^{N-1} \end{bmatrix} \tag{6}$$

$$\mathbf{C} = \begin{bmatrix} 1 & z_1^{-1} & \cdots & z_1^{-L+1} \\ 1 & z_2^{-1} & \cdots & z_2^{-L+1} \\ \vdots & \vdots & \ddots & \vdots \\ 1 & z_P^{-1} & \cdots & z_P^{-L+1} \end{bmatrix} \tag{7}$$

An eigenvalue decomposition is applied to the autocorrelation-like matrix $\mathbf{X}^H\mathbf{X}$, so that

$$\mathbf{X}^H\mathbf{X} = \mathbf{V}\Lambda\mathbf{V}^H \quad \text{with} \tag{8}$$

$$\mathbf{V} = \begin{bmatrix} v_1[1] & v_2[1] & \cdots & v_L[1] \\ v_1[2] & v_2[2] & \cdots & v_L[2] \\ \vdots & \vdots & \ddots & \vdots \\ v_1[L] & v_2[L] & \cdots & v_L[L] \end{bmatrix} \tag{9}$$

$$\Lambda = \begin{bmatrix} \lambda_1 & 0 & \cdots & 0 \\ 0 & \lambda_2 & \cdots & 0 \\ \vdots & \vdots & \ddots & \vdots \\ 0 & 0 & \cdots & \lambda_L \end{bmatrix} \tag{10}$$

and $\lambda_k = 0$ for $k = P+1, \ldots, L$ as the matrix $\mathbf{X}^H\mathbf{X}$ is of rank P. It can be shown, that any principal eigenvector $\mathbf{v}_k$ ($k = 1, \ldots, P$) of the matrix $\mathbf{X}^H\mathbf{X}$ is a linear combination of the columns of $\mathbf{C}^H$ (e.g. Marple, 1987), composed by the signal poles:

$$\mathbf{C}^H = \begin{bmatrix} 1 & 1 & \cdots & 1 \\ (z_1^*)^{-1} & (z_2^*)^{-1} & \cdots & (z_P^*)^{-1} \\ \vdots & \vdots & \ddots & \vdots \\ (z_1^*)^{-L+1} & (z_2^*)^{-L+1} & \cdots & (z_P^*)^{-L+1} \end{bmatrix}$$

Therefore, the columns of $\mathbf{C}^H$ are orthogonal to the non-principal eigenvectors $\mathbf{v}_k$ ($k = P+1, \ldots, L$).

In the presence of noise, the autocorrelation-like matrix of the signal plus noise can be approximated by

$$\mathbf{Y}^H\mathbf{Y} \approx \mathbf{X}^H\mathbf{X} + \sigma^2\mathbf{I} = \mathbf{X}^H\mathbf{X} + \sum_{k=1}^{L} \sigma^2 \mathbf{v}_k\mathbf{v}_k^H$$
$$= \sum_{k=1}^{P} (\lambda_k + \sigma^2)\mathbf{v}_k\mathbf{v}_k^H + \sum_{k=P+1}^{L} \sigma^2 \mathbf{v}_k\mathbf{v}_k^H. \tag{11}$$

with σ^2 the noise variance. The principal eigenvectors $\mathbf{v}_k$ ($k=1,\ldots,P$) expand the signal plus noise subspace and the eigenvectors $\mathbf{v}_k$ ($k=P+1,\ldots,L$) the noise subspace.

The MUSIC algorithm exploits the orthogonality between the noise subspace eigenvectors $\mathbf{v}_k$ and the columns of $\mathbf{C}^H$, the signal vectors

$$\mathbf{s}(z_p) = \left[1\ (z_p^*)^{-1} \cdots (z_p^*)^{-L+1}\right]^T \tag{12}$$

in different ways. The Spectral MUSIC looks for the peaks in the pseudospectrum $X(e^{j\omega})$

$$X(e^{j\omega}) = \frac{1}{D(e^{j\omega})} = \frac{1}{\mathbf{s}^H(e^{j\omega})\left(\sum_{k=P+1}^{L}\mathbf{v}_k\mathbf{v}_k^H\right)\mathbf{s}(e^{j\omega})} \tag{13}$$

which are at the signal frequencies and the Root-MUSIC algorithm obtains directly the roots of the null spectra polynomial $D(z)$:

$$D(z) = \sum_{k=P+1}^{L} V_k(z)V_k^*(1/z^*) \quad \text{with} \tag{14}$$

$$V_k(z) = v_k[1] + v_k[2]z^{-1} + \cdots + v_k[L]z^{-(L-1)} \tag{15}$$

Next, two possible extensions of this algorithm to the dualband case are presented.

3.2 Multiband radar signal processing

The radar response is sampled at two different subbands $\mathcal{B}_1$ and $\mathcal{B}_2$:

$$y[n] = \sum_{p=1}^{P} a_p z_p^n + w[n] \qquad \text{with} \tag{16}$$

$$n = \begin{cases} N_{10},\ldots,N_{10}+N_1-1 & \text{for } \mathcal{B}_1 \\ N_{20},\ldots,N_{20}+N_2-1 & \text{for } \mathcal{B}_2 \end{cases}$$

Two main approaches to treat the dualband case can be identified, the non-coherent approach, where no information on the band gap between the subbands is used and the coherent approach, where the information about the band gap is used in the algorithm.

3.2.1 Non-coherent multiband MUSIC

Using the data of the two subbands, a new data matrix is built by the superposition of the two subband matrices:

$$\mathbf{X}_{\text{nc}} = \begin{bmatrix}\mathbf{X}_1 \\ \mathbf{X}_2\end{bmatrix} \qquad \text{where} \tag{17}$$

$$\mathbf{X}_1 = \begin{bmatrix} x[N_{10}-L_1+1] & \cdots & X[N_{10}] \\ \vdots & \ddots & \vdots \\ x[N_{10}+N_1-1] & \cdots & x[N_{10}+N_1-L_1] \end{bmatrix} \tag{18}$$

$$\mathbf{X}_2 = \begin{bmatrix} x[N_{20}-L_2+1] & \cdots & X[N_{20}] \\ \vdots & \ddots & \vdots \\ x[N_{20}+N_2-1] & \cdots & x[N_{20}+N_2-L_2] \end{bmatrix} \tag{19}$$

and $L_1=L_2=L$. As in the single-band case, the matrix $\mathbf{X}_{textnc}$ can be decomposed into the product of the matrices $\mathbf{B}_{textnc}$ and $\mathbf{C}$, with

$$\mathbf{B}_{textnc} = \begin{bmatrix}\mathbf{B}_1 \\ \mathbf{B}_2\end{bmatrix} \tag{20}$$

and $\mathbf{C}$ defined as in Eq. (7). As the matrix $\mathbf{C}$ has the same structure as in the single-band case, the same procedure can be applied directly. No information of the band gap $N_{20}-N_{10}$ is used, therefore, no coherence between the two subbands is required.

3.2.2 Coherent multiband MUSIC

To exploit the relative position between the two subbands, a data matrix is built including the band-gap information in its structure.

$$\mathbf{X}_{textc} = \begin{bmatrix}\mathbf{X}_2\ \mathbf{X}_1\end{bmatrix} \tag{21}$$

where $\mathbf{X}_1$ and $\mathbf{X}_2$ are defined as in Eqs. (18) and (19), $L_1+L_2=L$ and $N_2-N_1=L_2-L_1$. The new data matrix $\mathbf{X}_{textc}$ is decomposed as the product of the matrices $\mathbf{B}$ and $\mathbf{C}_{textc}$, with $\mathbf{B}$ defined as in Eq. (6) and

$$\mathbf{C}_{textc} = \begin{bmatrix} 1 & \cdots & z_1^{-L_2+1} & z_1^{-\Delta N} & \cdots & z_1^{-\Delta N-L_1+1} \\ \vdots & \ddots & \vdots & \vdots & \ddots & \vdots \\ 1 & \cdots & z_P^{-L_2+1} & z_P^{-\Delta N} & \cdots & z_P^{-\Delta N-L_1+1} \end{bmatrix} \tag{22}$$

with $\Delta N = N_{20}-N_{10}+N_2-N_1$.

Comparing the structure of the data matrices for the single-band- $\mathbf{X}$, for the non-coherent dualband- $\mathbf{X}_{textnc}$ and for the coherent dualband-algorithm $\mathbf{X}_{textc}$, can be observed the difference of the approaches for analyzing the data. In the first two approaches, a window of length L is moved through the data set to characterize the relation between neighbor data samples with a maximum distance L between them. In the third approach, to build the data matrix $\mathbf{X}_{textc}$ the observation window is split into two sub-windows of length L_1 and L_2, each of them containing data from a different subband. This

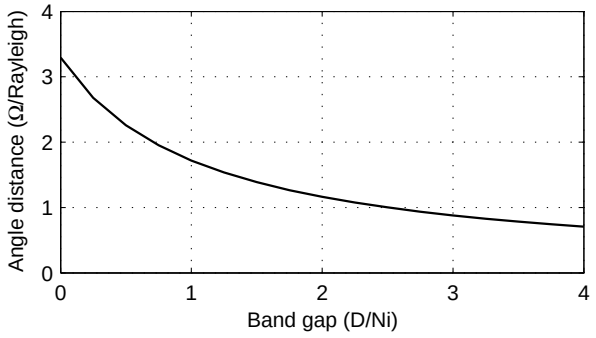

Fig. 1. Maximum resolvable angle distance using the non-coherent and coherent pole combination. Rayleigh angle distance is defined as $\frac{2\pi}{N_1+N_2}$.

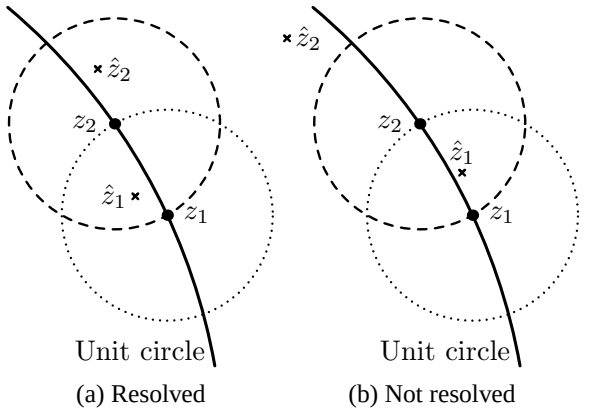

Fig. 2. Illustration of the resolution criteria: two targets are said to be resolved if the distances from the estimated poles ($\hat{z}_p$) to the true ones (z_p) is lower than the distance between the true positions.

window analyzes the relation between the neighbor samples in the same subband and the samples of the other subband.

Now, the noise subspace eigenvectors $\mathbf{v}_k$ are orthogonal to the columns of $\mathbf{C}_{textc}^H$, which are composed by the signal poles evaluated at the two subbands simultaneously

$$\mathbf{s}(z_p) = \left[1 \cdots (z_p^*)^{-L_2+1} (z_p^*)^{-\Delta N} \cdots (z_p^*)^{-\Delta N - L_1 + 1}\right]^T \quad (23)$$

The pole vectors which are orthogonal to the noise subspace, are identified again with two main procedures. The spectral MUSIC algorithm looks for the peaks in the pseudospectrum $X(e^{j\omega})$

$$X(e^{j\omega}) = \frac{1}{D(e^{j\omega})} = \frac{1}{\mathbf{s}^H(e^{j\omega}) \left(\sum_{k=P+1}^{L} \mathbf{v}_k \mathbf{v}_k^H\right) \mathbf{s}(e^{j\omega})}$$

and the root-MUSIC obtains the roots of the null spectra polynomial $D(z)$

$$D(z) = \sum_{k=P+1}^{L} V_k(z) V_k^*(1/z^*)$$

with the polynomial $V_k(z)$ evaluated at the two subbands:

$$V_k(z) = v_k[1] + \cdots + v_k[L_2] z^{-L_2+1} + v_k[L_2+1] z^{-\Delta N} + \cdots + v_k[L] z^{-\Delta N - L_1 + 1} \quad (24)$$

It is clear from the structure of the signal vectors $s(z_p)$ or the noise polynomials $V_k(z)$, that the information of the band gap is used and therefore, coherence is required. As the gap information ΔN is included directly in the null-spectra polynomial, the number of zeros of polynomial, i.e. the number of signal poles orthogonal to the noise subspace vectors, increases linearly with the band gap. This makes the distinction of the real signal poles from the spurious polynomial zeros difficult.

To overcome this problem, the information of the non-coherent and coherent algorithms is combined. Only the zeros of the coherent polynomial surrounding the zeros of the incoherent polynomial are analyzed. It is assumed, that the detection of a group of scatterers is achieved with the non-coherent approach, while with the coherent approach only an increase of resolution is expected. It may occur that two signal poles are present where the non-coherent approach detects only one. Assuming that the coherent polynomial zeros are approximately distributed uniformly along the unit circle, the maximum search distance to avoid spurious zeros is fixed by the total number of zeros, which is approximately equal to ΔN. This approach implies a limit in the maximum distance between two poles which can be still resolved with this algorithm as can be seen in Fig. 1.

4 Simulations

The resolution capability of the dualband processing has been assessed by means of simulations. Monte Carlo analysis of the probability of resolution, i.e. the frequency of experiments for which two targets are resolved over the number of experiments where two targets are present, have been carried out. A signal composed by two poles on the unit-circle with angular distance $\Delta\Omega$ between them and equal amplitude A buried in CWGN has been used as radar signal. The signal is sampled at two subbands with equal number of samples $N_1 = N_2 = 32$ and with a variable band gap of D samples between them. Both dualband root-MUSIC algorithms with $L = 8$ and $P = 2$ have been applied. As the number of expected targets P is assumed to be known in advance for the algorithm the number of detected targets can not be used as resolution criterion. The definition of resolution proposed here is illustrated in Fig. 2, two targets are said to be resolved if the distance between the estimated poles and the true ones is smaller than the distance between the true positions.

In Fig. 3 results of the Monte Carlo analysis for different angular distances between the poles $\Delta\Omega$ and signal to noise

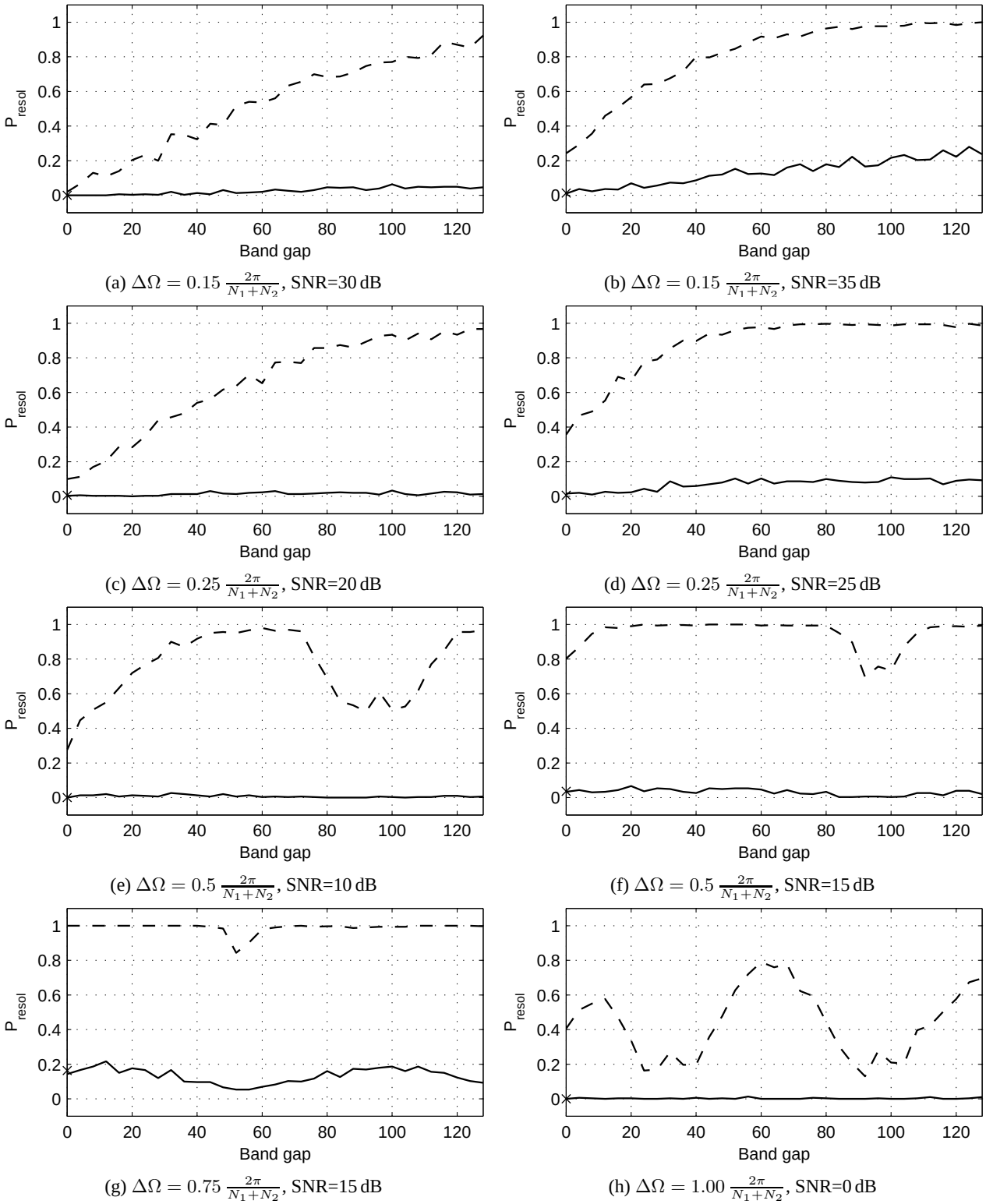

(a) $\Delta\Omega = 0.15\,\frac{2\pi}{N_1+N_2}$, SNR=30 dB

(b) $\Delta\Omega = 0.15\,\frac{2\pi}{N_1+N_2}$, SNR=35 dB

(c) $\Delta\Omega = 0.25\,\frac{2\pi}{N_1+N_2}$, SNR=20 dB

(d) $\Delta\Omega = 0.25\,\frac{2\pi}{N_1+N_2}$, SNR=25 dB

(e) $\Delta\Omega = 0.5\,\frac{2\pi}{N_1+N_2}$, SNR=10 dB

(f) $\Delta\Omega = 0.5\,\frac{2\pi}{N_1+N_2}$, SNR=15 dB

(g) $\Delta\Omega = 0.75\,\frac{2\pi}{N_1+N_2}$, SNR=15 dB

(h) $\Delta\Omega = 1.00\,\frac{2\pi}{N_1+N_2}$, SNR=0 dB

Fig. 3. Probability of resolution Monte Carlo analysis. Radar signal composed by two poles on the unit-circle with angular distance between them of $\Delta\Omega$, sampled at two subbands with $N_1 = N_2 = 32$ and with a band gap between them of D samples. Applied algorithms: Dualband root-MUSIC non-coherent (solid line), coherent (dashed line) with $L = 8$ and $P = 2$ and single-band ($\times$) with $N = N_1 + N_2 = 64$. The resolution event is defined as in Fig. 2.

ratio, defined as $\mathrm{SNR} = A^2/\sigma^2$, are shown. Also several single-band simulations with $N = N_1 + N_2 = 64$ have been carried out. The cases with a probability of resolution around 50% have been selected for demonstration.

It can be seen, e.g. Figs. 3f or 3g, that the dualband non-coherent approach has resolution performance similar to the single-band case. The non-coherent approach is therefore a robust way to exploit the whole bandwidth of a signal, also if the signal information is split in different, non-adjacent and mutually incoherent subbands $\mathcal{B}_{\mathrm{eq}} = \sum \mathcal{B}_i$.

The coherent approach achieves a higher probability of resolution. For low angle distances, $\Delta\Omega < 0.5\,\frac{2\pi}{N_1+N_2}$ from Figs. 3a to 3d, the improvement in the dualband coherent algorithm increases continuously with the band gap. Also an increase is observed in the dualband non-coherent approach (Fig. 3a). For greater pole distances however, the probability of resolution shows a periodic behavior with period $\approx \frac{2\pi}{\Delta\Omega}$. This is again observed in both dualband approaches. The origin of this periodicity effect will be subject of further investigations.

5 Summary and outlook

A signal model for the multiband radar response based on GO and GTD has been presented. Based on this model, it can be seen that the range estimation using frequency-domain radar information is analog to the spectral or frequency estimation techniques for time-domain signals. The MUSIC algorithm for spectral estimation has been extended to obtain two ways to process the multiband case: non-coherent and coherent. The non-coherent algorithm does not require coherency between the subbands. It does not use the band gap information and the resolution performance is similar to the single-band case using the sum of the bandwidths. It is therefore a robust approach to exploit the total bandwidth of a signal, also if the signal information is split in different, non-adjacent and mutually incoherent subbands. The coherent algorithm exploits the band gap information and therefore, coherent data sets are required. An increase in the resolution performance compared to the non-coherent algorithm is achieved. Also a periodic effect with period $\approx \frac{2\pi}{\Delta\Omega}$ for $\Delta\Omega > 0.5\frac{2\pi}{N_1+N_2}$ has been observed, which will be subject of further investigations.

References

Hansen, R. C.: Geometric Theory of Diffraction, IEEE Press, New York, 1981.

James, G. L.: Geometrical Theory of Diffraction for Electromagnetic Waves, Peter Peregrinus, Stevenage, Herts, England, revised third edn., 1986.

Marple, S.: Digital Spectral Analysis, Prentice Hall, Englewood Cliffs, New Jersey, 1987.

McNamara, D. A., Pistorius, C., and Malherbe, J.: Introduction to the Uniform Geometrical Theory of Diffraction, Artech House, Boston London, 1990.

Schmidt, R. O.: Multiple Emitter Location and Signal Parameter Estimation, IEEE Transactions on Antennas and Propagation, AP-34, 1986.